Possibility to link the seismic process of a megathrust earthquake with a cellular automaton

Hiroyuki Kikuchi[1]

[1]Seismic Lab

November 23, 2022

Abstract

This paper paves the way for a direct comparison of the process of megathrust earthquakes with cellular automaton (CA) and for modeling the catastrophic singularity of seismic events as a phase transition phenomenon. It is shown that the entropy production rate (EPR), which is a property of thermodynamically non-equilibrium systems, occasionally decreases sharply in the seismic process of the Great East Japan Earthquake (GEJE) of magnitude 9. The timing of the EPR decrease is found to be clearly different from that of earthquakes of magnitude less than 9, but close to the timing of the earthquake of magnitude 9. The decrease indicates a qualitative change from a time-dependent non-equilibrium system towards a static equilibrium system, which can be a phase transition. In the GEJE process, EPR is calculated from the binarized velocity deviation of ground vibrations found to be equivalent to velocity. The equivalence attributes to that the transformation between them does not change the α-tremor which is the curvature of the Fourier amplitude spectrum of the velocity, and that an arbitrary ground vibration can be defined by α-tremor. The α-tremor is a noise. However, it is associated with microearthquakes whose epicenter is close to the GEJE epicenter, and is an important component of the GEJE process. The binarization equivalence allows the ground vibration to be viewed as CA which consists of binary numbers.

Possibility to link the seismic process of a megathrust earthquake with a cellular automaton

Hiroyuki Kikuchi[1]*

[1]Seismic Lab, 307, 12-1, 2-Chome, Wakamiya, Okegawa-shi, Saitama 363-0022, Japan

Key Points:

- Weak ground vibration signals are binarized without losing Fourier spectral characteristics
- Thermodynamic state of ground motion is defined by the binarized signal
- State transition rate matrix and entropy production rate are evaluated from the thermodynamic states

*307, 12-1, 2-Chome, Wakamiya, Okegawa-shi, Saitama 363-0022, Japan

Corresponding author: Hiroyuki Kikuchi, hkikuchi@kkh.biglobe.ne.jp

Abstract

This paper paves the way for a direct comparison of the process of megathrust earthquakes with cellular automaton (CA) and for modeling the catastrophic singularity of seismic events as a phase transition phenomenon. It is shown that the entropy production rate (EPR), which is a property of thermodynamically non-equilibrium systems, occasionally decreases sharply in the seismic process of the Great East Japan Earthquake (GEJE) of magnitude 9. The timing of the EPR decrease is found to be clearly different from that of earthquakes of magnitude less than 9, but close to the timing of the earthquake of magnitude 9. The decrease indicates a qualitative change from a time-dependent non-equilibrium system towards a static equilibrium system, which can be a phase transition. In the GEJE process, EPR is calculated from the binarized velocity deviation of ground vibrations found to be equivalent to velocity. The equivalence attributes to that the transformation between them does not change the α-tremor which is the curvature of the Fourier amplitude spectrum of the velocity, and that an arbitrary ground vibration can be defined by α-tremor. The α-tremor is a noise. However, it is associated with microearthquakes whose epicenter is close to the GEJE epicenter, and is an important component of the GEJE process. The binarization equivalence allows the ground vibration to be viewed as CA which consists of binary numbers.

Plain Language Summary

This paper paves the way for a direct comparison of the process of megathrust earthquakes with cellular automaton (CA) and for modeling the catastrophic singularity of seismic events as a phase transition phenomenon. It is shown that the entropy production rate (EPR), which is an indicator of how much a vibration system changes with time, occasionally decreases sharply in the seismic process of the Great East Japan Earthquake (GEJE) of magnitude 9. The decrease indicates a qualitative change from a time-dependent non-equilibrium system towards a static equilibrium system, which can be a phase transition. EPR is calculated from the digitized velocity of ground vibration represented by "0" and "1". The digitized velocity is found to be equivalent to the undigitized velocity in the GEJE process. The equivalence attributes to the fact that the conversion between them does not change the α-tremor which is the curvature of the Fourier spectrum of the velocity, and that any ground vibration can be defined by α-tremor. The binarization equivalence allows the ground vibration to be viewed as CA which consists of binary numbers.

1 Introduction

Strong earthquakes are a major concern in disaster management, and various measures are being taken for strong earthquakes. Earthquake Early Warning system in Japan warns people when an earthquake of 5 or greater is expected on the Japan seismic scale. When an earthquake is detected, the system analyzes the data captured by seismographs near the epicenter to estimate the epicenter, the magnitude of the earthquake and the seismic intensity. The estimated information is quickly released so that people can move to safe places or evacuate from dangerous places before strong surface waves arrive. Regarding building regulations, the seismic standards of the Building Standard Law in Japan require minor damage in medium-scale earthquakes with a seismic intensity of 5 or greater, and no collapses in large-scale earthquakes with a seismic intensity of 6 to 7.

On the other hand, earthquakes generally last less than a minute, and the dominant state of ground motion is seismically silent. Therefore, in order to understand the seismic process, it is necessary to investigate the silent state. Nonvolcanic tremor is one of the notable discoveries regarding the silent state. Obara investigated the seismically silent period in southwest Japan and identified the nonvolcanic tremor, the weak but no-

ticeable signal with typical frequency range from 1 Hz to 10 Hz (Obara, 2002). Obara discussed that tremor with a long duration time is possibly caused by a chain reaction of small fractures induced by fluid. In 2003, Rogers and Dragert related tremors to ground slip events. Tremor activity accompanied by a slip event was observed approximately every 12 months for 6 consecutive years at Cascadia subduction zone interface (Rogers & Dragert, 2003). Regarding the mechanism of the long duration tremor, Peng and Chao observed the tremor induced by an earthquake and discussed that tremor occurred as a simple frictional response to the driving force (Peng & Chao, 2008).

This study focuses on the weak ground vibrations of micron/second scale in the seismic process of the Great East Japan Earthquake (GEJE), and represents the weak ground vibrations as α-tremors defined in a frequency range similar to the characteristic frequency range of nonvolcanic tremors. Then, the invariance of α-tremor is shown in the transformation from velocity to deviation velocity and in the transformation from velocity to binarized velocity deviation. The binarized velocity deviation and the raw velocity signal are considered as equivalent as long as the ground vibration is considered as a α-tremor fluctuation. Subsequently, vibrational states are defined by the binarized velocity deviation, and the stochastic dynamics of transition of the state in a Markov process are described by the master equation. Then, entropy production rate (EPR) is calculated from the dynamic parameters for the data recorded at the seismic station KSN, 188 km from the GEJE epicenter. Finally, the seismological significance of α-tremor is discussed in comparison to the microearthquake which occurred near the timing of α-tremor.

2 Observation of ground vibration signals

Ground vibration velocity data acquired every 0.05 seconds at the seismic station KSN is downloaded in chronological order from the web site of F-net, broadband seismograph network of National Research Institute for Earth Science and Disaster Resilience (NIED, 2019). The data is converted to piecewise deviation. Each section consists of 10 velocity data, and the piecewise deviation is the difference between the velocity within the section and the average velocity within the section. The piecewise deviation fluctuates around zero, and its squared average is the dispersion in statistics. The piecewise deviation data is divided into blocks of 1024 data, which corresponds to the data acquisition time of 51 seconds, and the Fourier amplitude of each block is calculated. The Fast Fourier Transform (FFT) algorithm is applied with no overlap, and no filtering. The upper bound of the frequency domain is 10Hz, which is half the data acquisition frequency. The lower bound is 0.02 Hz which is determined by the block size 1024. Therefore, the FFT with the sampling frequency of 20Hz and the block size of 1024 is equivalent to an FFT with a 0.02-10 Hz bandpass filter.

Fig. 1 shows a comparison of the velocities and spectrograms in the up-down (UD), north-south (NS), and east-west (EW) direction. The velocity data was acquired at KSN every 0.05 seconds from Mar. 3, 2011 to March 11, 2011. The period includes the magnitude 9 Great East Japan Earthquake (GEJE) occurred at 14:46 on March 11, 2011. In the spectrogram range from 1 Hz to 10 Hz, there are noticeable signals shown as the vertical brown lines. In the quiet period before the earthquake of magnitude 7.3, the timing of the vertical brown lines in the spectrograms (Fig. 2 (a4), (b2), and (c2)) respectively matches the timing of the wave clusters which have larger amplitude than surroundings (Fig. (a3), (b1), and (c1)). Since the UD component contains greater number of vertical brown lines than the other components, we focus on the UD component in the later sections.

The third brown line in Fig. 1 (a4), which corresponds to the velocity deviation in Zone_A in Fig. 1 (a3), constructs a finer spectrogram structure. Fig. 2 shows the details of the Zone_A of 12500 second duration. The velocity deviation and its spectrogram

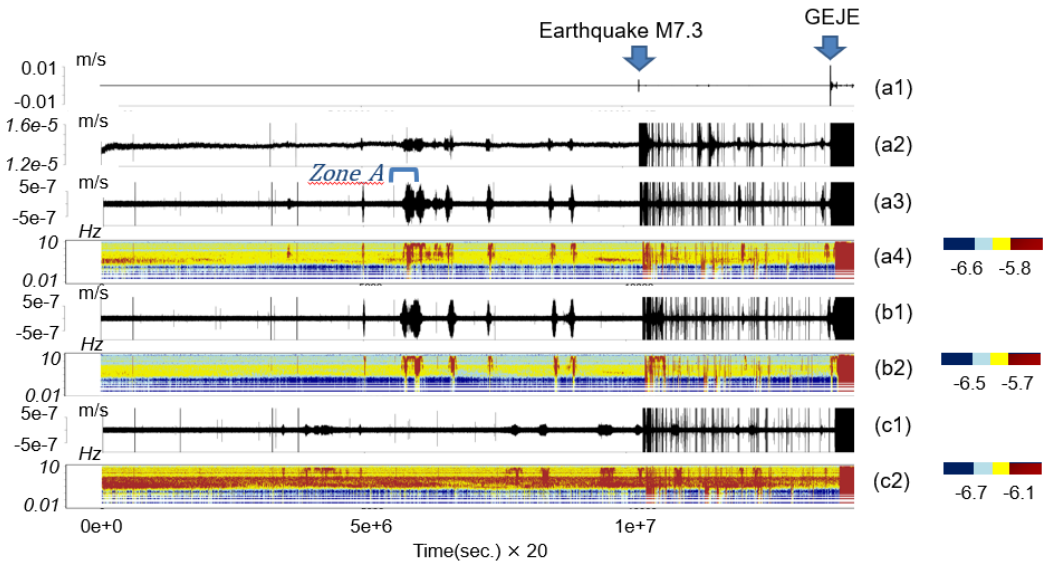

Figure 1: Ground vibration signals at KSN during March 3, 2011 to March 11,2011 period . (a1) Ground velocity (m/s) in UD direction. (a2) Magnified plot of (a1). (a3) Piecewise deviation of (a2). (a4) Spectrogram of (a3). (b1) Piecewise velocity deviation in NS direction. (b2) Spectrogram of (b1). (c1) Piecewise velocity deviation in EW direction. (c2) Spectrogram of (c1).

are shown in Fig. 2 (a) and 2 (b), respectively. Fourier amplitude spectrum and its 10 moving averages are respectively indicated by the black and red lines in the Log10-Log10 plots of Fig. 2 (c1) to 2 (c6). The spectrogram is plotted from the 10 moving averages. The velocity deviations in Fig. 2 (d1) to 2 (d6) are the source data for the amplitude spectrum. The number below the velocity deviation graph indicates the time interval (seconds x 20). The velocity deviations are extracted from the beginning, center, end, and their intermediates of the period shown in Fig. 2 (a), and are chronologically exhibited from left to right. The first and last amplitude spectra show small negative curvatures in the range 1 Hz to 10 Hz (Fig. 2 (c1) and 2 (c6)). The rest of the spectra show large values and negative curvatures in the range from 1 Hz to 10 Hz (Fig. 2 (c2) to 2 (c5)). The curvature widens in the center of the zone and narrows in the rest of the zone. The amplitude of the velocity deviation is small at the beginning and end, and large in the central zone.

3 Definition of α-tremor

The curvature of the Fourier amplitude spectrum is defined as the ratio of $P_{ni}-P_i$ to $|P_2-P_1|$ in Fig. 3 (a), where P_i is the point of the (frequency, spectrum) coordinate system. The frequency of P_1 and P_2 are 2.97 Hz and 9.8 Hz, which correspond to the 152th and 502th point on the frequency axis, respectively. The average of the spectrum value of the nearest 5 points are assigned as the spectrum value for the P_1 and P_2. P_i is a point in the 2.97-9.8 Hz range. P_{ni} is determined so that the line from P_i to P_{ni} is perpendicular to the line connecting P_1 and P_2. If the spectrum value of P_i is greater than that of P_{ni}, the curvature is negative. Otherwise, the curvature is non-negative. The curvature is independent of the scale change since the line length in log10 plot is invariant to the scalar multiplication of the coordinate values.

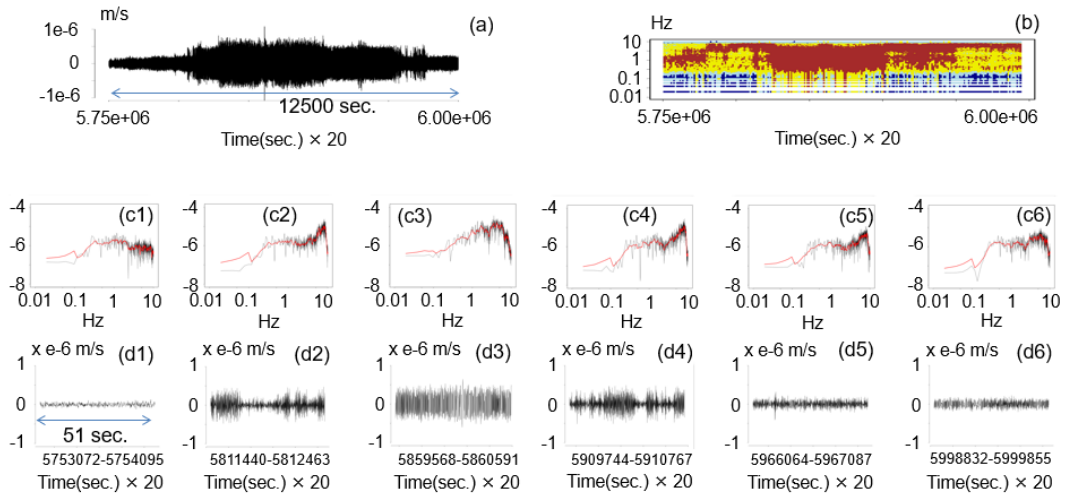

Figure 2: Fine structure of the signal in the Zone_A in Figure 1 (a3). (a) UD velocity deviation (m/s). (b) Spectrogram of (a). (c1)-(c6) Fourier amplitude spectrum excerpted from (b). (d1)-(d6) UD velocity deviation, the source data for (c1)-(c6).

We define α-tremor as the product of "-1" and the curvature of which absolute value is greater than the absolute value of other curvatures in the frequency range of 2.97 to 9.8 Hz (Fig. 3 (a)). An arbitrary ground velocity signal is classified as either positive α-tremor or non-positive α-tremor.

The α-tremor for the velocity data acquired at KSN during March 03, 2011 to March 11, 2011 is exhibited in Fig. 3 (b). As expected, the positive peak of the α-tremor appears at a timing similar to the brown line in Fig. 1 (a4).

It should be noted that the piecewise velocity deviation is equivalent to the raw velocity data in evaluating the α-tremor. Fig. 4 (a) compares the Fourier amplitude spectrum of the velocity deviation data to the amplitude spectrum of the raw velocity data. In the range of 2.97 Hz to 9.8 Hz, the amplitude spectrum of the deviation velocity (black line) matches the spectrum of the raw data (green line) by 80%. Therefore, we may select either the piecewise deviation velocity data or the raw velocity data to obtain a unique amplitude spectrum in the range 2.97 Hz to 9.8 Hz. The orange and red lines in Fig. 4 (a) are the 10-moving averages of the black and green lines, respectively. The source data of the spectrum, which are the velocity deviation and velocity acquired at KSN during the period from March 1, 2012 to March 10, 2012, are shown in Fig. 4 (b) and 4 (c), respectively.

4 Binarization of velocity deviation data

The velocity deviation data is binarizable without losing the α-tremor property. In Fig. 5, the Fourier amplitude spectrum and spectrogram calculated from the velocity deviation are compared to those calculated from the binarized velocity deviation. Fig. 5 (a1) and 5 (b1) shows the binarization procedure. If each velocity deviation data in Fig. 5 (a1) is greater than the mean of the data set under consideration, the deviation data is converted to 1, otherwise the deviation data is converted to 0. The binarized data can be expressed as the time sequence of 0 and 1 as shown in Fig. 5 (b1). The clear negative curvature in the frequency range 1 Hz to 10 Hz, shown in both the Fourier spectrum of the velocity deviation and the binarized data, implies that the α-tremor is pre-

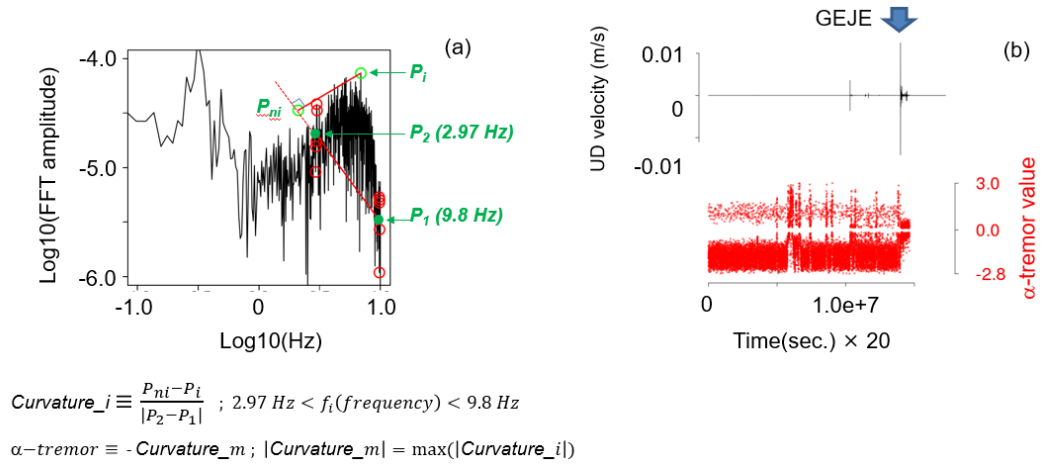

Figure 3: Definition of α-tremor. (a) Definition of spectrum curvature and α-tremor. (b) α-tremor calculated for the UD velocity data of $Fig.1(a1)$.

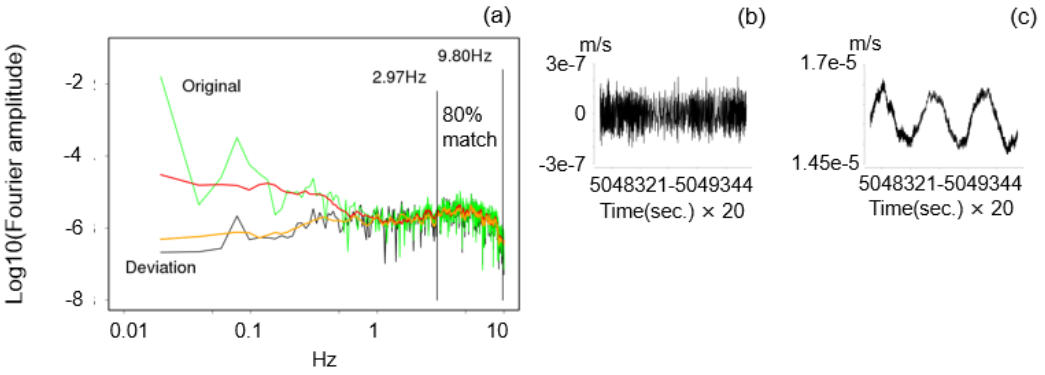

Figure 4: Comparison of velocity deviation spectrum and velocity spectrum, which have negative curvatures. Spectrums of ground vibration signals recorded at KSN during the period from March 1, 2012 to March 10, 2012. (a) Fourier amplitude spectrum of velocity in the UD direction, and spectrum of deviation velocity. (b) UD velocity deviation data. (c) UD velocity data.

served in the binarization (Fig. 5 (a2) and (b2)). Fig. 5 (a3) is the Fourier amplitude spectrogram duplicated from Fig. 2 (b), of which source data is the velocity deviation shown in Fig. 2 (a). The source data is binarized and its spectrogram is calculated as shown in Fig. 5 (b3). The qualitative similarity between the spectrogram of the binarized data and the spectrogram of the source data suggests that the α-tremor is preserved in the binarization (Fig. 5 (a3) and (b3)). Therefore, the binarized velocity and velocity deviation are equivalent as long as the ground vibration is considered as a α-tremor fluctuation.

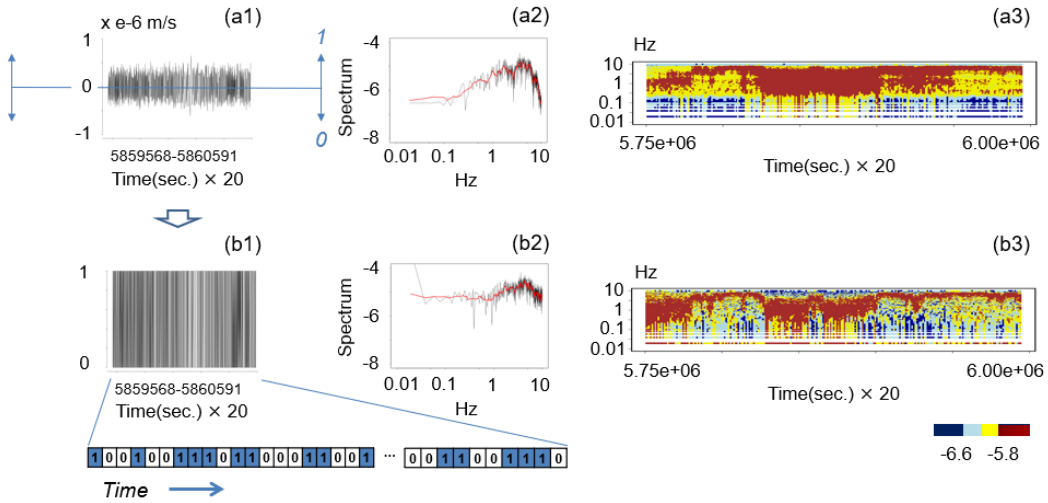

Figure 5: Binarization of velocity deviation. (a1) Velocity deviation duplicated from *Fig*.2(*d*3). (a2) Fourier amplitude spectrum of (a1). Duplicate of *Fig*.2(*c*3). (a3) Fourier amplitude spectrogram of the velocity deviation recorded at KSN during 5.75e6 to 5.6e6 (sec x 20). The time origin is 00:00 on March 3, 2011. Duplicate of *Fig*.2(*b*). (b1) Binarization result of (a1). (b2) Fourier amplitude spectrum of (b1). (b3) Fourier amplitude spectrogram of the binarized velocity deviation recorded at KSN during 5.75e6 to 5.6e6 (sec x 20). The time origin is 00:00 on March 3, 2011. Compare with (a3).

5 Definition of ground vibration state

Since the α-tremor is conserved in the binarization of the velocity signal, the essential of the ground motion is the distribution of the signal rather than the shape of the signal. Therefore, it is reasonable to define the ground vibration state in a specified time interval by counting the cluster of 1 in the interval of the binarized velocity. In defining the vibration state, the binarized velocity sequence (Fig. 6 (a)) is divided into blocks with 10 data points, and the number of clusters of "1" is counted in each block. In order to preserve the total number of the cluster, the rule shown in Fig. 6 is applied. In the 10-data block, we scan the cell from left to right and count one if the sequence of "10" is found. At the end of the scan, at the 10th data point, we count one only if the 11th data point is "0" (Fig. 6 (b)). The counting rule restricts the maximum number of clusters in a block to five, and defines five vibrational states s_1, s_2, s_3, s_4 and s_5, each containing 1, 2, 3, 4, and 5 clusters (Fig. 6 (c1)- 6 (c5)).

The number of data points 10 per block is determined by examining samples of binarized velocity data. If a block of a particular size is completely occupied by 1s, then the number of clusters of 1s in the block is 1. If this is the case for all blocks, no fluctuation in state can be detected. The block size needs to be increased to detect the characteristics of the state. If the blocks are very large and each block contains all possible patterns of 0s and 1s, then all the blocks will look similar and no fluctuation of state will be detected. In this case, the block size must be reduced. After examining a few cases, it is found that the 10 data points per block is adequate to preserve the characteristic of the state change.

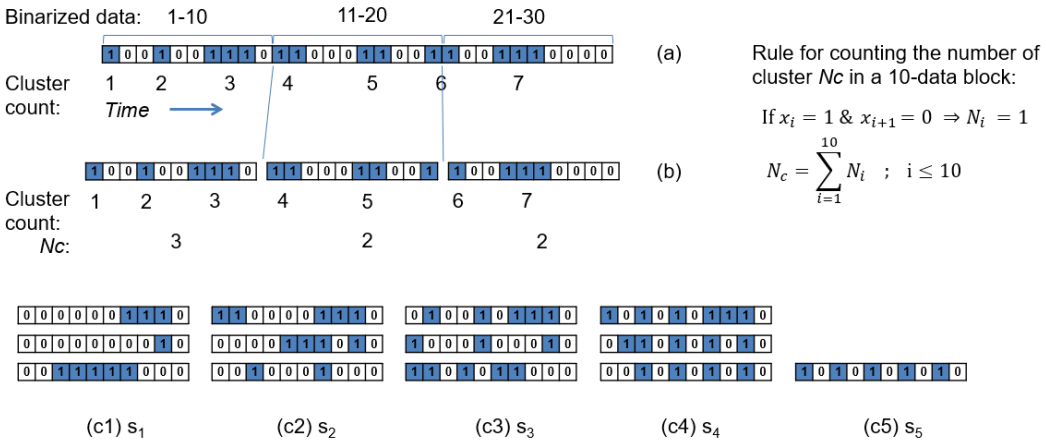

Figure 6: Definition of ground vibration state. (a) Sequence of binarized velocity deviations and counts of "1" clusters. (b) Blocks with 10 data points divided from the sequence in (a), and counts of "1" clusters. (c1)-(c5) Examples of the ground vibration state s_1, s_2, s_3, s_4, and s_5, each containing 1, 2, 3, 4, and 5 clusters.

6 Thermodynamics of the ground vibration

Fig. 7 (a) shows the first 100 data of the binarized velocity deviation data of Fig. 5 (b1). The 10 data in each row of Fig. 7 (b) are the binarized velocity deviation data splitted from Fig. 7 (a), and constitute the vibration state with a time interval of 0.5 seconds. In general, the vibration state shows a different pattern of binary sequence for each row and contains a different number of clusters for each row (Fig. 7 (c)). Since each row corresponds to a different time, the state of ground vibration fluctuates over time.

The time series of the number of clusters in Fig. 7 (c) shows the history of the state transitions. Since the number of clusters in a state is defined as a state index, the square brackets that make up the pair of two numbers indicate that the state of the number in the lower row has transitioned to the state of the number in the upper row. The transition rate matrix W_{ij} defines the total number of transitions from i-state to j-state so that the W_{ij} count is incremented by 1 when a transition from i-state to j-state occurs (Fig. 7 (d)). The result of the W_{ij} counting for the 100 data is shown in Fig. 7 (e). Fig. 7 (f) shows the probability density vector, of which component p_i is the total number of i-state.

The state of ground vibration, which fluctuate over time, implies that the state is non-equilibrium. It is known that the thermodynamics of a fluctuating nonequilibrium system are described by the master equation (Eq. (1)), and the entropy production rate (Eq. (2)) which is similar to the entropy of the second law of thermodynamics of equilibrium systems (Haitao, Y. & Jiulin, D., 2014).

$$\frac{dp_i}{dt} = \sum_{j=1}^{n} J_{ij}(t) \tag{1}$$
$$J_{ij}(t) = W_{ij}(t)p_j(t) - W_{ji}(t)p_i(t)$$
$$F_{ij}(t) = ln\frac{W_{ij}(t)p_j(t)}{W_{ji}(t)p_i(t)}$$

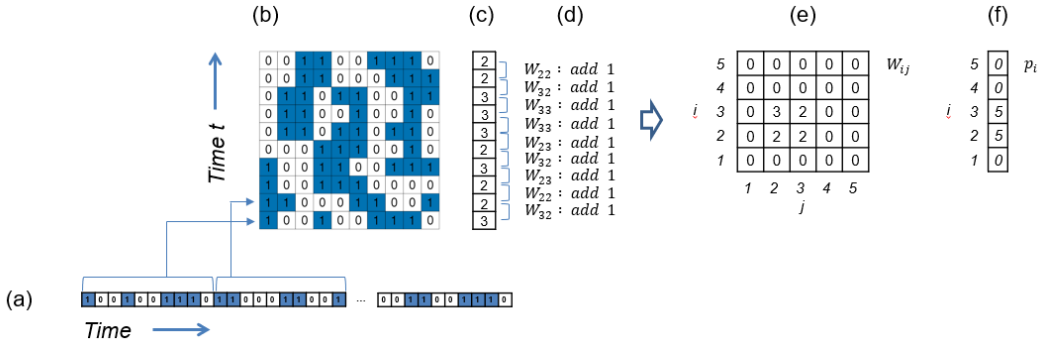

Figure 7: Transition rate matrix and probability density of state. (a) The first 100 data of the binarized velocity deviation data of $Fig.5(b1)$. (b) A pile of blocks containing 10 data points divided from (a). (c) The number of clusters in the block, or the index "i" of the vibration state s_i. Chronological transition sequence from the lower state s_i to the upper state s_j. (d) The procedure for calculating W_{ij}, which is a component of the transition rate matrix. (e) W_{ij} calculated for (c). (f) Probability density distribution of states in the 100 data in (c). The numbers are not normalized. p_i is the total number of the states s_i in the 100 data.

$$\sigma(t) = \frac{1}{2}\sum_{i=1}^{n}\sum_{j=1}^{n} J_{ij}(t)F_{ij}(t) \tag{2}$$

where W_{ij} and p_i are coherent with those in Fig. 7. J_{ij} and F_{ij} are called the flow from i-state to j-state and thermodynamic force, respectively.

Fig. 8 shows EPR, the Fourier amplitude spectrum, W_{ij} contour plot, and the vibration states in the first 10 time steps. These are calculated from the binarized data of the velocity deviation in Fig. 2 (d1) -2 (d6). Small positive α-tremors, or small negative curvatures in the spectrum from 2.97 to 9.8 Hz, tend to be accompanied by a small EPR (Fig. 8 (a1) and 8 (a6)).

7 Thermodynamics in the process of GEJE

EPR, α-tremor, and earthquakes at KSN during the seismic process of GEJE from January 1, 2006 to December 31, 2018 are compared in Fig. 9. Fig. 9 (a) shows the location of KSN and the measuring point of the seismic intensity, epicenter of the earthquakes A,B,C,and D occurred during the period. The earthquake B is the GEJE of magnitude 9. The table in Fig. 9 includes the identifiers of earthquakes, date, magnitude, seismic intensity, and the epicenter of the earthquakes searched on the website of the Japan Meteorological Agency of Ministry of Land, Infrastructure, Transport and Tourism (JMA-1, 2019). The search conditions are the seismic intensity greater than 4, the location of observing the seismic intensity, and the time period for search. For UD velocity data acquired every 0.05 seconds at KSN, EPR is calculated every 10 days and plotted in Fig. 9 (b). Fig.9 (c) shows the time evolution of α-tremor, which is calculated every 51.2 seconds for the UD velocity data.

From the beginning of 2006 to the end of 2007 (0 to 730 days), the EPR fluctuates stably between 0.050 and 0.065, which indicates a stable nonequilibrium thermodynamic state. The positive α-tremor is monotonously distributed and does not show a peak.

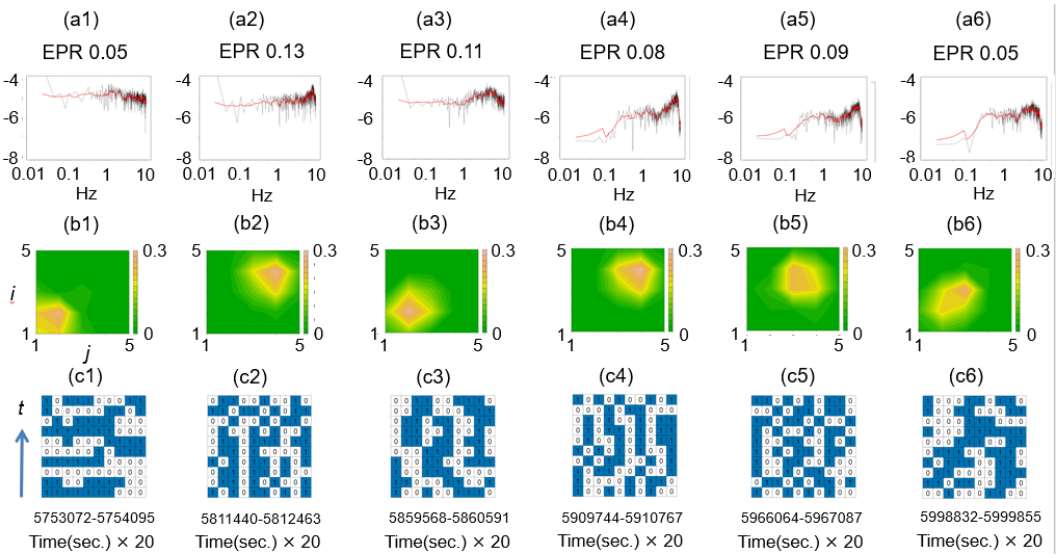

Figure 8: Thermodynamics of the ground vibration signal in the Zone_A in $Fig.1(a3)$. Corresponds to $Fig.2$. (a1)-(a6) EPR and Fourier amplitude spectrum calculated from the binarized data of the velocity deviation in $Fig.2(d1) - 2(d6)$. (b1)-(b6) W_{ij} contour plot. (c1)-(c6) Vibration states in the first 10 time steps.

From the beginning of 2008 to the end of 2014 (731 to 3285 days), EPR occasionally decreases to a minimum of 0.03. The timing of the EPR decrease is the same as the strong peak of positive α-tremor. Since the state of $EPR = 0$ corresponds to the equilibrium state in which no state transition occurs, the positive α-tremor peak indicates the state change toward the thermodynamic equilibrium state. Unlike α-tremor, EPR decrease is clearly asymmetric with respect to the timing of GEJE. The bottom of EPR gradually decreases from 2008 to 2011 when GEJE occurred, but stays around 0.03 from 2011 to 2014.

From the beginning of 2015 to the end of 2016 (3286 to 4015 days), EPR recovers to the stable nonequilibrium level between 0.050 and 0.065, and no positive α-tremor peak is observed.

During the period from the beginning of 2017 to the end of 2018 (4016 to 4745 days), the EPR occasionally decreases to around 0.04 at the timing of the vivid α-tremor peak. However, no decrease in EPR is observed at the relatively weak α-tremor peak near 4000 days.

Either the positive α-tremor peak or decrease in EPR does not coincide with the timing of earthquakes A, C and D. The α-tremor and the EPR, which are characteristics of micron-scale vibrations, are often independent of large earthquakes of magnitude 6.8 to 7.2. On the other hand, the timing of GEJE (earthquake B of magnitude 9) is close to both the positive α-tremor peak and the EPR decrease, so a megathrust earthquake may be associated with micron-scale vibrations.

To understand the distinguishing features of the seismic process of a megathrust earthquake, EPR, α-tremor and earthquake are compared for the data recorded at the seismic station TMC, which is 1170 km away from the GEJE epicenter, during the period from 2008 to 2018 (Fig. 10). During most of the period, EPR fluctuates stably between 0.05 and 0.065, and EPR does not decline sharply, while 4 earthquakes of mag-

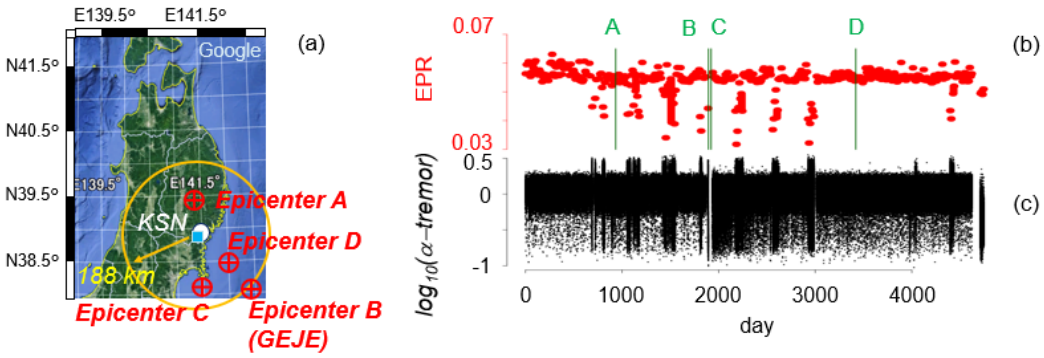

ID	Date	Magnitude	Seismic Intensity	Latitude	Longitude	Depth(km)
A	Jul. 24, 2008	6.8	5	39.43*N*	141.38*E*	108
B	Mar. 11, 2011	9	6	38.06*N*	142.51*E*	24
C	Apr. 07, 2011	7.2	5	38.12*N*	141.55*E*	66
D	May 13, 2015	6.8	5	38.52*N*	142.09*E*	46

Figure 9: EPR, α-tremor and earthquakes at KSN during the seismic process of GEJE from 2006 to 2018. For the earthquakes with a seismic intensity greater than 4, the identifier, time, magnitude, seismic intensity, and location are listed in the table. The capital letters A, B, C, and D are earthquake identifiers and correspond to the IDs in the table. (a) The location of the KSN (white filled circle), epicenter (red plus-circle) of the earthquake, and the seismic intensity measurement point (blue filled square). The seismic intensity is recorded at Kesennuma-city, approximately 10 km from KSN, which is 188 km from the GEJE epicenter. (b) EPR. The green line indicates the timing of the earthquake identified by the uppercase letter at the top of the line. (c) Positive α-tremor. The start and end of the elapsed time are 2006-01-01 00:00 and 2018-12-31 23:59, respectively.

nitude 5.9 to 7.3 are observed near TMC. The positive α-tremor is monotonously distributed and does not show a strong peak. It is consistent with the KSN case that no sharp decline in EPR and no strong peak of α-tremor are observed at the timing of earthquakes of magnitude less than 9, and that the EPR from 0.05 to 0.065 corresponds to a stable nonequilibrium ground-vibration. In addition, there is no significant change in EPR and α-tremor at GEJE timing, suggesting that the distance of 1170 km distance is adequate to dampen the influence of GEJE.

8 Seismological significance of α-tremor

In the previous sections, we have investigated the fluctuation of ground such as α-tremor and EPR for the data recorded by F-net's broadband seismograph (NIED, 2019) installed at KSN and TMC. In order to understand the relation between the ground fluctuation and seismic events, the α-tremor is compared with the seismic spectra recorded by the high-sensitivity seismographs of Hi-net (NIED-2, 2019) consisting of nearly 800 stations with an average spacing of 20 km. The Hi-net seismographs are installed at the bottom of boreholes at a depth of 100-3500 m to reduce the noise generated by winds, ocean waves, and human activity. The natural frequency of the seismograph is 1 Hz. The locations of the three Hi-net seismic stations near the KSN, namely IWTH27, MYGH03, and IWTH18, are shown in Fig. 11.

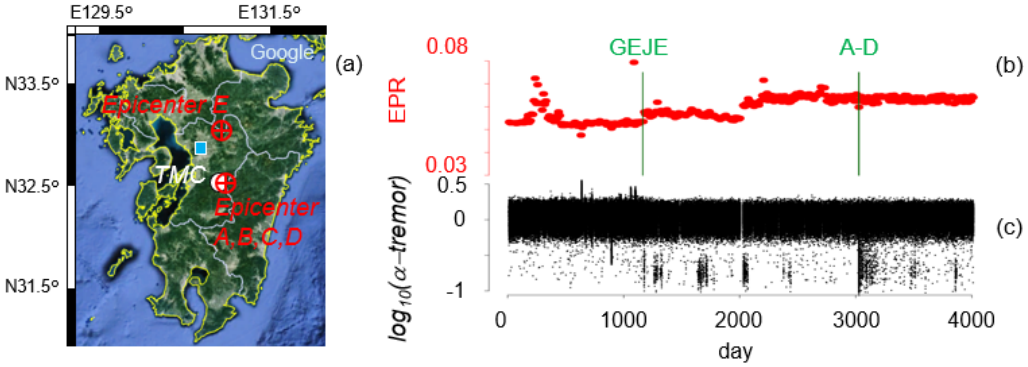

ID	Date	Magnitude	Seismic Intensity	Latitude	Longitude	Depth(km)
A	Apr. 14, 2016	6.5	5	32.44*N*	130.48*E*	11
B	Apr. 16, 2016	7.3	6	32.45*N*	130.45*E*	12
C	Apr. 16, 2016	5.4	5	32.45*N*	130.45*E*	15
D	Apr. 16, 2016	5.9	5	32.51*N*	130.53*E*	11

Figure 10: EPR, α-tremor and earthquakes from 2008 to 2018 at TMC, 1170 km away from the GEJE epicenter. For the earthquakes with a seismic intensity greater than 4, the identifier, time, magnitude, seismic intensity, and location are listed in the table. The capital letters A, B, C, and D are earthquake identifiers and correspond to the IDs in the table. (a) The location of the TMC (white filled circle), epicenter (red plus-circle) of the earthquake, and the seismic intensity measurement point (blue filled square). The seismic intensity is recorded at Kumamoto-kita-ku, approximately 39km from TMC. (b) EPR. The green line indicates the timing of the earthquake identified by the uppercase letter at the top of the line. (c) Positive α-tremor. The start and end of the lapsed time are 2008-01-01 00:00 and 2018-12-31 23:59, respectively.

The Fourier amplitude spectrum of the velocities recorded from 21:18 to 11 minutes on 2011/03/06 are compared between KSN and IWTH27 in Fig. 12. Since the two seismic stations are 6 km apart and close to each other, the signals arriving at the stations are similar. The negative curvature of the spectrum in the range 2.97 Hz to 9.8 Hz, α-tremor, is observed from 21:18 to 21:24 (blue rectangle in Fig. 12 (a1)). The velocity plots corresponding to α-tremor are relatively dense, as shown in the blue rectangle in Fig. 12 (a2). In this figure, we do not see seismic p-waves, seismic s-waves, and the nonvolcanic tremor that is detectable by plotting the envelope which is the root mean square trace of the 2 Hz-16 Hz bandpass-filtered velocity data (Obara & Hirose, 2006). Therefore, it is appropriate to think of α-tremor as a kind of noise signal rather than an earthquake or nonvolcanic tremor.

The α-tremor is excluded from Hi-net, and not found in the spectrum of IWTH27 (Fig. 12 (b1)). However, instead, Hi-net detects an earthquake from 21:26 to 21:27, one minute after the end of the series of α-tremor (Fig. 12 (b2)), suggesting a relation between α-tremor and the earthquake.

In order to understand α-tremor in terms of seismic events, microearthquakes occurred in the neighborhood of α-tremor are investigated. The top plot in Fig. 13 (a) shows two microearthquakes E1 and E2 in the seismogram recorded at Hi-net IWTH27 for 12540 seconds starting from 2011/03/06 20:18. The time range is similar to the range discussed in Fig. 2 (a) and (b), during which the clusters of α-tremor are observed at F-net KSN.

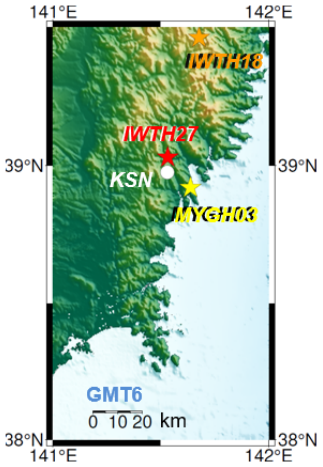

Figure 11: Seismic station. The filled red star, the filled yellow star, and the filled orange star are the seismic stations IWTH27, MYGH03, and IWTH18, respectively.

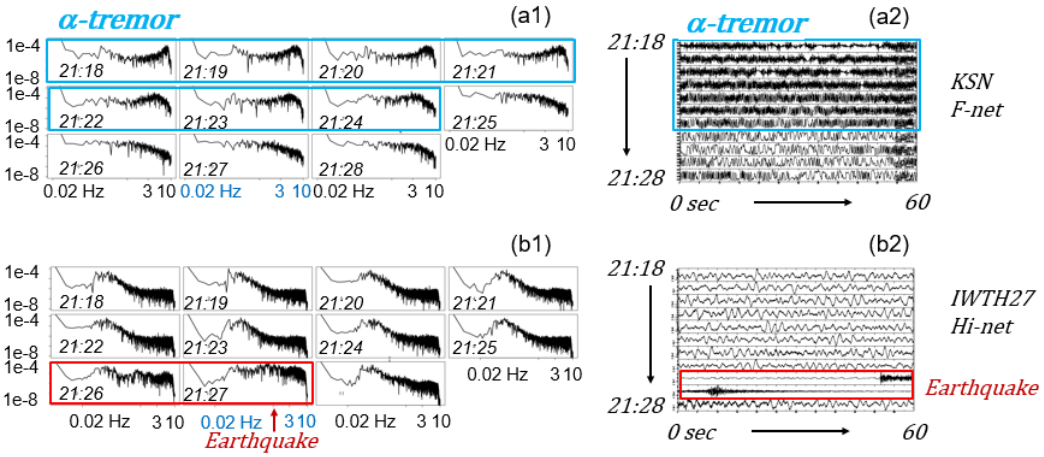

Figure 12: Comparison of velocity and spectrum between F-net KSN and Hi-net IWTH27. Elapsed time starts from 2011/03/06 21:18. The sampling frequencies for KSN and IWTH27 are 20 Hz and 100 Hz, respectively. (a1) Fourier amplitude spectrum of KSN. (a2) The velocity in UD direction. Source data of (a1). (b1) Fourier amplitude spectrum of IWTH27. (b2) UD velocity. Source data of (b1).

The microearthquake E1 is the earthquake occurred one minute after the end of the α-tremor cluster shown in Fig. 12 (a1). At the timing of E1 and E2, no earthquake is recorded at F-net KSN, as shown in the bottom plot in Fig. 13 (a).

By applying a bandpass filter in the range of 4 Hz to 9.5 Hz, relatively high-amplitude and low-amplitude clusters emerge in the F-net KSN seismogram (Fig. 13 (b) top). The first high-amplitude cluster corresponds to the first cluster of α-tremor in the middle plot of Fig. 13 (b). One minute after the end of the cluster, the microearthquake E1 occurs as shown in the bottom plot of Fig. 13 (b). It should be noted that the microearthquake E2 disappeared after applying the bandpass filter (bottom plot in Fig. 13 (b)). As shown in Fig. 13 (d1), E2 has no significant frequency component from 4 Hz to 9.5 Hz in the

Fourier amplitude spectrum. E2 has the frequency components primarily around 1 Hz, which is dissimilar to the α-tremor spectrum in Fig.12 (a1).

The Fourier amplitude spectrum of the microearthquake E1 shows that it has wide range of frequency components from 1 Hz to 10 Hz (Fig. 13 (c1)), which is qualitatively similar to the Fourier spectrum of α-tremor in Fig.12 (a1). The similarity in frequency components implies similarities in material composition, system size and dynamics between E1 and the α-tremor.

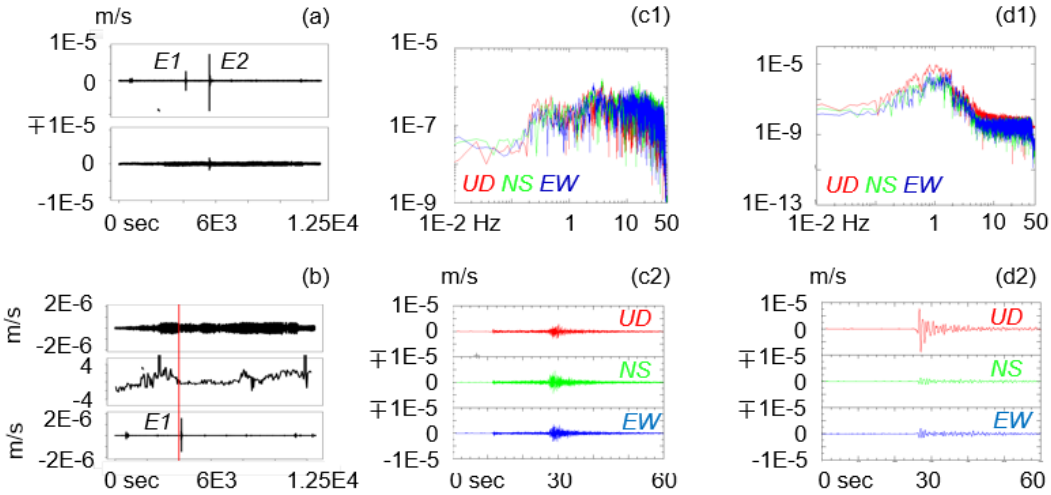

Figure 13: Micro earthquakes near α-tremor. (a) Top: UD Velocity at Hi-net IWTH27 for 12540 seconds starting from 2011/03/06 20:18. The time range is similar to the range discussed in Fig. 2 (a) and (b). Bottom: UD velocity at F-net KSN. (b) Top: The 4 Hz - 9.5 Hz bandpass-filtered UD Velocity at F-net KSN for 12540 seconds starting from 2011/03/06 20:18. Middle: The α-tremor calculated for the UD velocity at F-net KSN. Bottom: The 4 Hz - 9.5 Hz bandpass-filtered UD Velocity at Hi-net IWTH27.The vertical red line indicates the end time of the first α-tremor cluster. (c1) Fourier amplitude spectrum of the velocity of the microearthquake E1 shown in $Fig.13(a)$. The velocities in the UD, NS, and EW directions were recorded at Hi-net IWTH27 for 60 seconds from 21:26 on 2011/03/06. (c2) The source velocity data of (c1). (d1) Fourier amplitude spectrum of the velocity of the microearthquake E2 shown in $Fig.13(a)$. The velocities in the UD, NS, and EW directions were recorded at Hi-net IWTH27 for 60 seconds from 21:51 on 2011/03/06. (d2) The source velocity data of (d1).

Since the source velocity data of the E1 spectrum clearly shows p-wave and s-wave (Fig. 13 (c2)), the epicenter of E1 is estimated. The epicenter of E1 is graphically estimated as the intersection of three circles, which are defined by the radius D calculated by Omori's formula: $D = kT$, with the locations of three seismic stations as the origin. Where T is the difference between the arrival times of p-wave and s-wave at the station, and k is an empirical factor equal to 8 (Kato & Okamoto, 2016). Fig. 14 (a) shows that the estimated E1 epicenter is close to the GEJE epicenter, suggesting that E1 belongs to the events in the seismic process of GEJE.

In summary, the α-tremor is a noise, but it occurs one minute before the microearthquake E1 and has the Fourier frequency component similar to E1 whose epicenter is close to the GEJE epicenter. Consequently, α-tremor is an important constituent factor of the seismic process of GEJE.

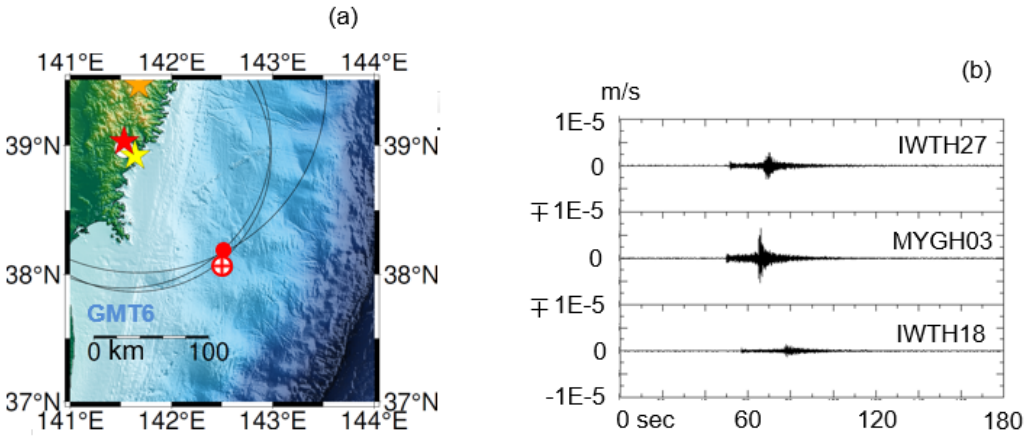

Figure 14: Estimate of the epicenter of the E1 earthquake. (a) Estimated epicenter of E1 (red filled circle), epicenter of GEJE (plus circle), the three Hi-net seismic stations considered in the estimation, and the KSN. (b) UD velocity recorded at the three stations for 180 seconds from 2011/03/06 21:26. Top: Recorded at IWTH27, Middle: MYGH03, and Bottom: IWTH18.

9 Conclusions

In order to analyze the thermodynamic changes in the ground vibration state during the seismic process of GEJE, EPR and α-tremor are evaluated from the binarized velocity deviation of weak ground vibrations. The binarized data is equivalent to the raw velocity data since both data yield the same α-tremor, and since the ground vibration can be represented by α-tremor. It is worth noting that due to the equivalence in the binarization, the ground vibration can be regarded as a cellular automaton consisting of binary numbers.

It is found that EPR occasionally decreases in the GEJE process, which indicates the qualitative ground-vibration state change from a time dependent nonequilibrium thermodynamic state towards a stable equilibrium state, which can be a phase transition.

The timing of the EPR decrease coincides with the timing of the strong positive peak of α-tremor. EPR and α-tremor are confirmed as important constituents of the GEJE process since EPR decrease is observed at the timing close to the GEJE event, and since α-tremor is associated with the microearthquake whose epicenter is close to the GEJE epicenter.

Acknowledgments

Data is publicly available through National Research Institute for Earth Science and Disaster Resilience, National Research and Development Corporation under Ministry of Education, Culture, Sports, Science and Technology. F-Net (Broadband seismograph network) data base. http://www.fnet.bosai.go.jp/top.php?LANG=en.

References

Obara, K. (2002). Nonvolcanic Deep Tremor Associated with Subduction in Southwest Japan. Science 31 May 2002: Vol. 296, Issue 5573, pp. 1679-1681. DOI: 10.1126/science.1070378

Rogers, G. & Dragert, H. (2003). Episodic Tremor and Slip on the Cascadia Subduction Zone: The Chatter of Silent Slip. Science 20 Jun 2003: Vol. 300, Issue 5627, pp. 1942-1943. DOI: 10.1126/science.1084783

Obara, K. & Hirose, H. (2006). Non-volcanic deep low-frequency tremors accompanying slow slips in the southwest Japan subduction zone. Tectonophysics. 417. 33-51. doi:10.1016/j.tecto.2005.04.013.

Peng, Z. & Chao, K. (2008), Non-volcanic tremor beneath the Central Range in Taiwan triggered by the 2001Mw 7.8 Kunlun earthquake. Geophys. J. Int. (2008) 175, 825-829 doi: 10.1111/j.1365-246X.2008.03886.x

Haitao, Y. & Jiulin, D. (2014), Entropy Production Rate of Non-equilibrium Systems from the Fokker-Planck Equation. Braz J Phys 44, 410-414 (2014). https://doi.org/10.1007/s13538-014-0234-6

Kato, M. & Okamoto, Y. (2016). On Omori Coefficients for Distances and Their Use in Science Education. Earthquake No. 2, 2016, Vol. 69, p. 35-39. DOI: 10.4294/zisin.69.35

NIED (2019). National Research Institute for Earth Science and Disaster Resilience, National Research and Development Corporation under Ministry of Education, Culture, Sports, Science and Technology. F-Net (Broadband seismograph network) data base. DOI: 10.17598/nied.0005. http://www.fnet.bosai.go.jp/top.php?LANG=en

NIED-2 (2019). National Research Institute for Earth Science and Disaster Resilience, NIED Hi-net, National Research Institute for Earth Science and Disaster Resilience, doi:10.17598/NIED.0003.

JMA-1. (2019). Japan Meteorological Agency under Ministry of Land, Infrastructure, Transport and Tourism. Seismic intensity database search. https://www.data.jma.go.jp/svd/eqdb/data/shindo/index.php